

Oxidation dynamics of ultrathin GaSe probed through Raman spectroscopy

Alaric Bergeron,^{1, a)} John Ibrahim,¹ Richard Leonelli,² and Sebastien Francoeur^{1, b)}

¹⁾*Department of Engineering Physics, Polytechnique Montréal, Montréal H3T 1J4, Canada*

²⁾*Department of Physics, Université de Montréal, Montréal H3T 1J4, Canada*

Gallium selenide (GaSe) is a 2D material with a thickness-dependent gap, strong non-linear optical coefficients and uncommon interband optical selection rules, making it interesting for optoelectronic and spintronic applications. In this work, we monitor the oxidation dynamics of GaSe with thicknesses ranging from 10 to 200 nm using Raman spectroscopy. In ambient temperature and humidity conditions, the intensity of all Raman modes and the luminescence decrease rapidly with moderate exposure to above-gap illumination. Concurrently, several oxidation products appear in the Raman spectra: Ga₂Se₃, Ga₂O₃ and amorphous and crystalline selenium. We find that no safe measurement power exists for optical measurements on ultrathin GaSe in ambient conditions. We demonstrate that the simultaneous presence of oxygen, humidity, and above-gap illumination is required to activate this photo-oxidation process, which is attributed to the transfer of photo-generated charge carriers towards aqueous oxygen at the sample surface, generating highly reactive superoxide anions that rapidly degrade the sample and quench the optical response of the material.

Gallium selenide (GaSe) is a layered pseudo-direct gap semiconductor¹ with strong non-linear properties in the visible, IR and THZ ranges^{2,3}, a high photoreponse from 2 to 5 eV⁴, a highly anisotropic band structure exhibiting uncommon selection rules^{5,6}, and interesting spin physics⁷. Atomically thin GaSe can be mechanically exfoliated from bulk samples^{8,9} or grown by chemical vapor transport¹⁰. Its bulk band gap of 2.12 eV^{2,11} is predicted to increase to more than 3.5 eV for the monolayer^{12,13}. Atomically thin flakes and devices have shown a high photoresponse^{9,14}, a composition tunable band gap¹⁵, near-unity optical polarization¹⁶, the strongest second-harmonic generation observed in a monolayer 2D material^{17,18}, and transistors with high ON/OFF ratios¹⁹.

Like most 2D materials, the properties of GaSe are expected to sensitively depend on the interaction of its surface with its chemical environment. In bulk form, GaSe is generally considered as a stable material and is known to have a high laser damage threshold suitable for non-linear optics applications^{20,21}. Nonetheless, bulk GaSe is also known to naturally form a native oxide²² and thermally- and photo-induced oxidation has been reported²³⁻²⁵. Recently, exposure to intense laser light was found to degrade optical properties and lead to chemical transformations²⁶⁻²⁸. Given the interest for few-layer GaSe for electronic and optoelectronic applications, it appears critical to examine the oxidation dynamics of ultrathin GaSe and determine the conditions in which this oxidation can be suppressed or at least minimized.

In this paper, we monitor the complex oxidation dynamics of ultrathin GaSe and identify the emergence of several oxidation products using Raman spectroscopy. This oxidation, highly detrimental to all optical and electronic processes, requires the simultaneous presence

of oxygen, humidity, and above-gap illumination and is adequately described in the framework of the Marcus-Gerischer theory. We demonstrate that removing any of these three components greatly reduces the oxidation rate.

GaSe layers were mechanically exfoliated from Bridgeman-grown bulk crystals²⁹ using PDMS stamps onto silicon (Si) substrates covered with a 100 nm thermal oxide (SiO₂). Flakes with thicknesses ranging from 10 to 200 nm were identified by optical contrast using an optical microscope and their thickness was established from atomic force microscopy (AFM) measurements. Raman measurements were conducted in backscattering geometry using a 532 nm single-mode laser. The spatial and spectral resolution were 0.6 μm and 0.2 cm⁻¹, respectively. For sample in vacuum experiments, samples were exfoliated in a dry N₂-flushed environment and transferred to an optical cell evacuated to a pressure of 1.5 × 10⁻⁶ mTorr. Deoxygenated water vapor was obtained from deionized water subjected to several freeze-thaw cycles under vacuum. Experiments in oxygen were done using 99.999% O₂ gas (<3 ppm H₂O) at a partial pressure of 250 Torr. Finally, measurements in ambient air were done at a temperature of 23 °C and under a 48% relative humidity.

Raman spectra are used to monitor the integrity of thin GaSe layers and the appearance of photo-induced oxidation products. In this first experiment, samples were exposed to 6 mW μm⁻² of radiation at 532 nm, which corresponds to about 6% of the established laser damage threshold for nanosecond pulses at 620 nm³⁰. This illumination is about 230 meV above the bandgap of GaSe. Fig. 1 presents the evolution of the Raman spectrum as a function of exposure time for a 45 nm thick GaSe sample in air. Freshly exfoliated GaSe measured in vacuum (pristine GaSe) presents the usual dominant Raman modes expected from bulk GaSe^{29,31,32}: A₁¹ at 134 cm⁻¹, E₁¹(TO) at 214 cm⁻¹, and A₁⁴ at 308 cm⁻¹. Two other vibrational modes located at 236 cm⁻¹ and at 246 cm⁻¹ were often observed from pristine GaSe. These Raman

^{a)}Electronic mail: alaric.bergeron@polymtl.ca

^{b)}Electronic mail: sebastien.francoeur@polymtl.ca

modes are also associated to bulk GaSe^{29,31,32}, but they will not be considered in this work due to their much weaker intensity compared to A_1^1 , $E_1'(TO)$ and A_1^4 .

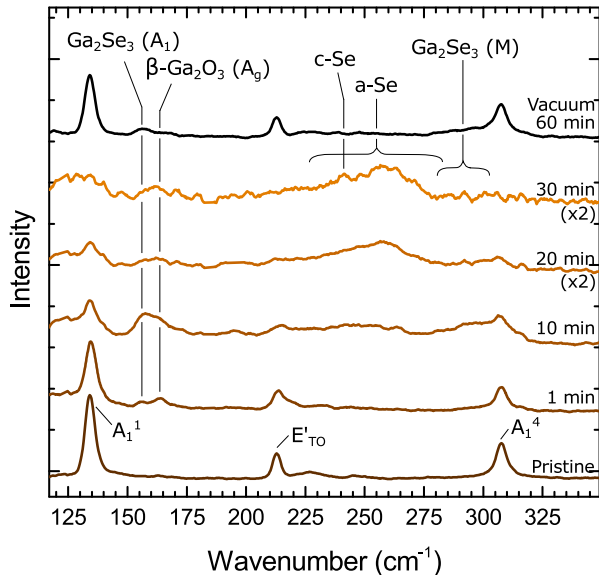


FIG. 1. Evolution of the Raman spectrum of a 45 nm-thick GaSe sample in air as a function of exposure time to a $6 \text{ mW } \mu\text{m}^{-2}$ radiation at 532 nm. Pristine refers to a second sample measured in vacuum immediately after exfoliation; the topmost curve is a spectrum obtained after 60 min of $6 \text{ mW } \mu\text{m}^{-2}$ exposure in vacuum of the same sample. In the experiment, the temperature increase induced by the exposure light is estimated at less than 40 K

The Raman spectrum evolves significantly as a function of exposure time. The intensity of all features associated with GaSe rapidly decreases and several additional Raman modes appear at frequencies of 155 cm^{-1} , 161 cm^{-1} , 257 cm^{-1} and 282 cm^{-1} . All GaSe vibrational modes are already accounted for^{31,32} and none of these additional features can be related to any of the various known GaSe polytypes. They are attributed to a photo-induced chemical transformation of GaSe and corresponds to well-known thermal oxidation products: Ga_2Se_3 , a-Se, $\beta\text{-Ga}_2\text{O}_3$ (see §SI in Supplementary Material for a description of the three main thermal oxidation pathways and their activation temperatures).

The frequency and width of the first mode at 155 cm^{-1} corresponds to the vibrational mode A_1 of Ga_2Se_3 ³³. Although Ga_2Se_3 exhibits several Raman-allowed modes, the one at 155 cm^{-1} is the narrowest and most intense³³⁻³⁵ and thus the more likely to be observed. Ga_2Se_3 has a defect zinc-blende structure in which Ga vacancies may or may not be ordered. The polarization-resolved Raman measurements presented in Fig. S1(a) in Supplementary Material suggest that the photo-induced $\alpha\text{-Ga}_2\text{Se}_3$ phase is polycrystalline. Another feature related to Ga_2Se_3 is observed at 292 cm^{-1} after a 10 min photoexposure. This broad ($\sim 10 \text{ cm}^{-1}$) feature actually corresponds to a group of at least three

vibrational modes with various symmetry representations (A_1 , B_1 , B_2) that have been assigned to localized vibrational modes of vacancy-disordered Ga_2Se_3 ³⁴. For its connection with multiple vibrational modes, this feature is labeled Ga_2Se_3 (M). Its presence suggests a high level of disorder in the Ga_2Se_3 phase.

After exposure of 20 min and more, the Raman signal is dominated by two even broader features. The first at 130 cm^{-1} likely corresponds to SeO_2 or SeO_3 Raman modes^{36,37}, but a quantitative analysis of this feature has proven difficult; it will not be further discussed. The other feature at 257 cm^{-1} matches the characteristics of a mode associated to selenium^{26,38} and its width ($\sim 20 \text{ cm}^{-1}$) suggests an amorphous phase (a-Se)^{39,40}. The narrower peak ($\sim 5 \text{ cm}^{-1}$) at 241 cm^{-1} appears last and is associated⁴¹ to a selenium crystalline phase (c-Se). As it has been often demonstrated, a-Se easily photo-crystallizes^{42,43}.

The feature observed at 161 cm^{-1} does not correspond to any modes belonging to GaSe, $\alpha\text{-Ga}_2\text{Se}_3$, or Se and its oxides. However, its frequency and width match the characteristics of the A_g vibrational mode of $\beta\text{-Ga}_2\text{O}_3$ ^{44,45}. According to Ref. 45, this feature should be the second most intense Raman feature from $\beta\text{-Ga}_2\text{O}_3$; the most intense one, found in single crystals at 199 cm^{-1} , has not been unambiguously observed in this work. Polarization-resolved data is presented in Fig. S1(b) in the Supporting Information.

The formation of these oxidation products is monitored as a function of time through the intensity of their Raman modes. Fig. 2 (a) shows that the relative integrated intensity of all GaSe modes (A_1^1 , E_{TO}' , A_1^4) rapidly decreases with time. After 25 min of exposure, relative Raman intensities have dropped to $\sim 15\%$ of their initial values, revealing that the integrity of the GaSe layer is severely compromised by photo-induced oxidation mechanisms. The luminescence intensity measured at 620 nm also rapidly decreases (see Fig. S2 in the Supplementary Material).

Fig. 2 (b) shows the integrated intensity of the oxidation products. After only one minute of exposure, the intensity of these modes is substantial and easily measurable. $\alpha\text{-Ga}_2\text{Se}_3$ (A_1) and Ga_2Se_3 (M) increase to a maximum value after 5-10 min and then decrease below the detection limit after 30 min. $\beta\text{-Ga}_2\text{O}_3$ (A_g) appears and then retains a relatively constant intensity throughout the oxidation process. In contrast, the intensity of a-Se rapidly increases and eventually plateaus at an intensity significantly higher than that of all other observed Raman modes, as can be seen in Fig. 1.

Direct oxidation of GaSe into Ga_2O_3 and Se has been shown to dominate at low temperatures^{22,46,47} and, after complete oxidation involving high temperatures, only Ga_2O_3 and elemental selenium should remain⁴⁸ (see §SI of Supplementary Material). The rapid initial increase in intensity of all modes associated to Ga_2Se_3 , Ga_2O_3 and Se suggests that more than one oxidation pathway is activated and that thermal oxidation is not the dominant

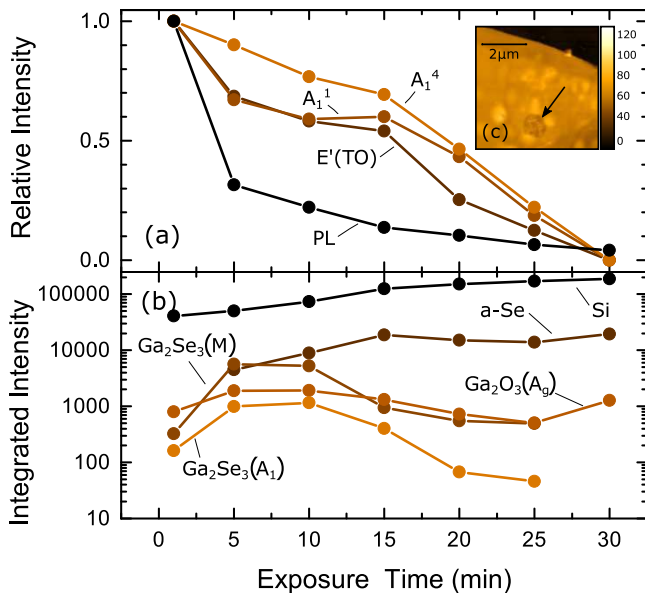


FIG. 2. Integrated Raman intensity and luminescence as a function of exposure time of a 45 nm thick GaSe flake in air. (a) Relative intensity of GaSe Raman modes and photoluminescence. (b) Integrated intensity of Raman modes associated to the oxidation products and Silicon. (c) AFM surface profile (color scale in nm) of the laser damage on a 58 nm thick flake after 30 min of 6 mW laser exposure. A black arrow indicates the ~ 12 nm deep, sharply defined hole caused by the laser induced oxidation.

mechanism due to the low temperatures involved. As detailed in §II of the supplementary material, the temperature increase occurring in the experiment presented in Figs 1 and 2 is less than 40 K.

The Raman intensity is proportional to the quantity of material in the probed volume, but it is also sensitive to its structural quality. It is therefore difficult to establish the concentrations of crystalline oxidation products, as, for example, the decrease of both Ga_2Se_3 modes could be related to its oxidation into Ga_2O_3 (see §SI of the Supplementary Material) or to the degradation of its crystalline structure as the oxidation progresses. During oxide formation, excess Se segregates at the surface²². As seen from Fig. 2(b), its intensity quickly increases at short exposure times and mirrors the drop of intensity of GaSe Raman modes and luminescence signal. Because its response is much less sensitive to its structural quality, $a-Se$ is believed to be the most reliable Raman marker of oxidation amongst the various products (see also §V in Supplementary Material).

The Raman signal from the Si substrate located underneath the GaSe flake steadily increases with time even though the excitation conditions are rigorously controlled. This is explained by the generation of a large-gap oxide and localized ablation. Oxidation leads to the formation of $\beta-Ga_2O_3$ with a gap of 4.9 eV⁴⁹, which is transparent at the excitation energy of 2.33 eV. Also, post-exposure AFM measurements indicate a layer-by-

layer thinning induced by the laser exposure (see Fig. 2 (c)). This is explained by the high volatility of Se and the high atomic mobility of the remaining metallic Ga³⁵. As a net result, the absorption from the GaSe flake decreases.

As suggested by the data presented in Fig. 1 (topmost curve), placing the sample in a vacuum environment protects GaSe samples from photo-induced oxidation. Curve A presented in Fig. 3 shows the evolution of the A_1^1 Raman intensity of a 10 nm thick flake as a function of time for an excitation power of 250 μW . For such thin layers, this power yields a weak but measurable Raman signal. The intensity of GaSe Raman modes is only marginally affected after an exposure of more than 60 min in vacuum. At the time indicated by the vertical dashed line, the sample was exposed to ambient air. After a few minutes, the Raman intensity has dropped by two orders of magnitude and the signal is completely lost after 10 min. This clearly shows that thin GaSe flakes are unstable in ambient conditions and that minimal laser illumination is sufficient to induce significant degradation, establishing that no safe above-gap excitation power exists for atomically-thin samples.

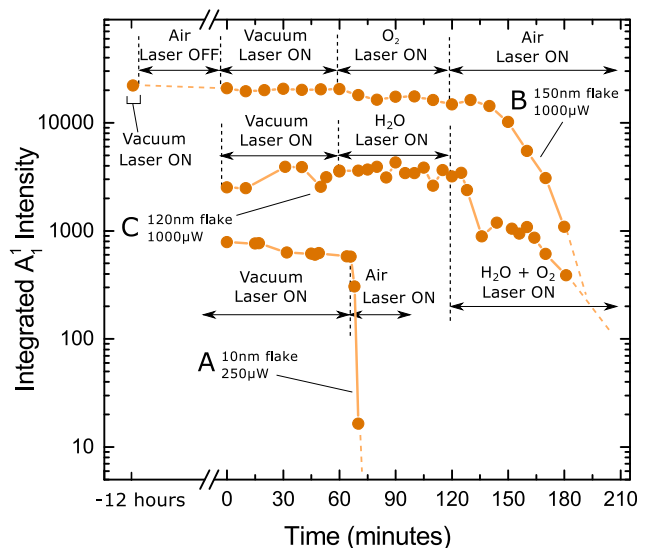


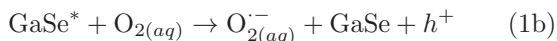
FIG. 3. Integrated Raman intensity of the A_1^1 peak of GaSe flakes as a function of exposure time to a 532 nm laser in vacuum and in different environments. Flake thickness and exposure power are indicated on the curves.

Curve B presented in Fig. 3 shows the Raman intensity of A_1^1 of a 150 nm flake exposed to 1000 μW of laser intensity. For the first data point, the sample is in vacuum. The sample is then exposed to ambient air without any illumination. After 12 hours, the sample is again measured under vacuum conditions and the Raman intensity is very similar to that initially measured, indicating that exposure to oxygen and water vapor alone does not induce significant chemical changes. After 60 min of laser illumination in vacuum, no appreciable change in intensity is

observed, even though residual H_2O is present in the sample chamber and on the sample. Then, dry oxygen (<3 ppm H_2O) is introduced in the optical cell and the sample is exposed to radiation for another 60 min. A slight change in Raman intensity is observed, but the overall signal loss is minor because of the limited amount of H_2O available at the sample. Finally, the sample is exposed to ambient air and continually illuminated for another 60 min. It takes about 15 min for the intensity to change significantly. This delay is attributed to a relatively slow nucleation and initial growth of degradation by-products for thicker samples. From that point on however, a rapid decline of intensity takes place, losing more than one order of magnitude within less than one hour. Curve C in Fig. 3 shows the Raman intensity from a 120 nm flake measured in vacuum and then in deoxygenated water vapor. The Raman intensity does not show any appreciable change after 1 hour in each environment. Introduction of oxygen in the chamber at the 120 min mark leads to a rapid decrease in the Raman intensity. These experiments establish that continuous above-gap illumination, water vapor and oxygen alone do not support the photo-oxidation process, but that the simultaneous presence of all three is required.

Although the observed oxidation byproducts are those observed from thermally-activated oxidation (Eqs. (S1a)-(S1c) in the Supplementary Material), the photo-oxidation process observed in this work is not temperature driven. The Raman shifts observed correspond to a temperature variation of at most 43 K at the studied exposure powers (see §SII in the Supplementary Material for the detailed analysis). This result confirms that the above gap illumination is not contributing significant heat, but rather generating an carrier density $\delta\eta$ in the conduction band.

The results presented thus far suggest that the photo-oxidation involves these three steps: optical excitation of carriers, electron transfer towards aqueous (aq) oxygen molecules at the surface of the sample, and spontaneous reaction between aqueous oxygen superoxide anions ($\text{O}_{2(aq)}^-$) with the p -doped semiconductor. This process can be modeled using the following equations:



where GaSe^* represents GaSe with photoexcited electron hole pairs, and $\{\text{GaSe}\}_{\text{ox}}$ represents GaSe oxidation byproducts. Although the photo-driven dynamics are expected to be quite different from the thermal dynamics discussed in Ref. 46, our results confirm that the oxidation byproducts are similar.

The charge transfer between the photo-excited carriers and aqueous oxygen (Eq. (1b)) can be understood in the framework of the Marcus-Gerischer theory, where the

rate of charge transfer is described by⁵⁰⁵⁰ :

$$\frac{d[\text{O}_{2(aq)}^-]}{dt} \propto \delta\eta[\text{O}_2] \exp \left[-\frac{(\chi_{\text{GaSe}} - E_{F,redox}^0 - \lambda)^2}{4k_B T \lambda} \right], \quad (2)$$

where $\delta\eta$ is the conduction band electron density, $[\text{O}_2]$ and $[\text{O}_{2(aq)}^-]$ are the concentrations of neutral oxygen and superoxide in the water at the sample surface, χ_{GaSe} is the GaSe electron affinity, $E_{F,redox}^0$ is the Fermi level of the oxygen-water solution and λ is the solvent reorganization energy around oxygen molecules. Since GaSe has an electron affinity which positions the lower conduction band in line with the aqueous oxygen acceptor states, the exponential function in Eq. 2 enables charge transfer towards the aqueous O_2 (see §SVI in the supplementary material). The generated aqueous superoxide anions ($\text{O}_{2(aq)}^-$) at the surface then rapidly react with the p -doped GaSe (Eq. (1c)) to produce the observed oxidation byproducts, which will in turn decrease the observed GaSe Raman intensity.

In the thickness regime studied here, the band gap variation is negligible,^{12,13} and the absorption coefficient is independent of thickness. The rate at which superoxide anions are generated is thus proportional to the exposure power, $d[\text{O}_{2(aq)}^-]/dt \propto \delta\eta \propto P_{\text{exp}}$. Fig. 4 shows the intensity of A_1^1 obtained after an exposure of 15 min at the indicated exposure power in ambient air for samples of varying thicknesses. As predicted by Eq. (2), the observed degradation rate increases linearly with exposure power and is independent of sample thickness, as evidenced from the very similar slopes measured. This confirms the role of the linear dependence of the photo-oxidation mechanism on above gap illumination and further rules out thermal processes.

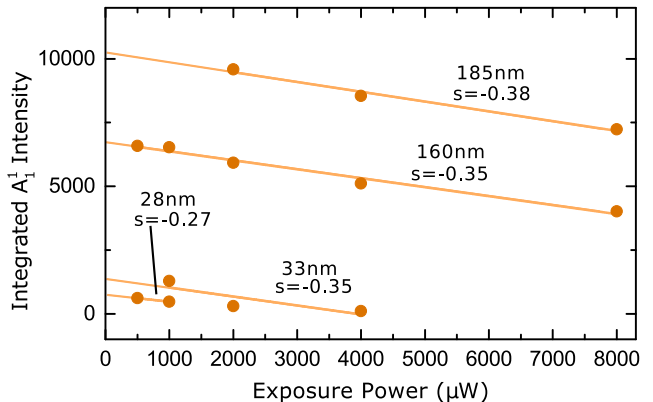


FIG. 4. Integrated Raman intensity of A_1^1 as a function of exposure power for samples of varying thicknesses. Each data point represents a 15 min exposure at the specified power before a Raman spectrum was measured using a $500 \mu\text{W}$ laser excitation. Linear regression slopes s are shown.

In summary, GaSe exhibits a relatively complex oxidation dynamics compared to other 2D materials. It

involves several components : oxygen, humidity, and above-gap illumination, and results in the generation of several oxidation products, Ga_2Se_3 , Ga_2O_3 and amorphous and crystalline selenium. Luminescence and Raman measurements in ambient conditions are found to severely degrade the optical and electronic characteristics of GaSe, indicating that no safe illumination threshold exists, especially for thin layers of GaSe. Hence, the study of the intrinsic characteristics of 2D GaSe requires a controlled environment at all stages of processing and characterization.

See supplementary material for more detail on the thermal oxidation process and thermal effects, for further analysis of the polarized Raman spectra of the oxide products and of sample photoluminescence, and for additional information regarding the role of water vapor and oxygen in the oxidation process.

This work was made possible by funding from the Fonds de Recherche du Québec-Nature et Technologie (FRQNT) and the Natural Sciences and Engineering Research Council of Canada (NSERC).

- ¹S. Nagel, A. Baldereschi, and K. Maschke, *Journal of Physics C: Solid State Physics* **12**, 1625 (1979).
- ²K. R. Allakhverdiev, M. Ö. Yetis, S. Özbek, T. K. Baykara, and E. Y. Salaev, *Laser Physics* **19**, 1092 (2009).
- ³K. C. Mandal, S. H. Kang, M. Choi, J. Chen, X.-C. Zhang, J. M. Schleicher, C. A. Schmuttenmaer, and N. C. Fernelius, *IEEE Journal of Selected Topics in Quantum Electronics* **14**, 284 (2008).
- ⁴C. H. Ho, M. H. Hsieh, and C. C. Wu, *Review of Scientific Instruments* **77**, 113102 (2006).
- ⁵W. Y. Liang, *Journal of Physics C: Solid State Physics* **8**, 1763 (1975).
- ⁶N. Kuroda and Y. Nishina, *Physica B+C* **105**, 30 (1981).
- ⁷A. N. Starukhin, D. K. Nelson, and B. S. Razbirin, *Journal of Experimental and Theoretical Physics* **111**, 645 (2010).
- ⁸D. J. Late, B. Liu, H. S. S. R. Matte, C. N. R. Rao, and V. P. Dravid, *Advanced Functional Materials* **22**, 1894 (2012).
- ⁹P. Hu, Z. Wen, L. Wang, P. Tan, and K. Xiao, *ACS nano* **6**, 5988 (2012).
- ¹⁰S. Lei, L. Ge, Z. Liu, S. Najmaei, G. Shi, G. You, J. Lou, R. Vajtai, and P. M. Ajayan, *Nano letters* **13**, 2777 (2013).
- ¹¹E. Aulich, J. L. Brebner, and E. Mooser, *Physica Status Solidi (C)* **31**, 129 (1969).
- ¹²D. V. Rybkovskiy, N. R. Arutyunyan, A. S. Orekhov, I. A. Gromchenko, I. V. Vorobiev, A. V. Osadchy, E. Y. Salaev, T. K. Baykara, K. R. Allakhverdiev, and E. D. Obraztsova, *Physical Review B* **84**, 085314 (2011).
- ¹³P. Hu, L. Wang, M. Yoon, J. Zhang, W. Feng, X. Wang, Z. Wen, J. C. Idrobo, Y. Miyamoto, D. B. Geohegan, and K. Xiao, *Nano letters* **13**, 1649 (2013).
- ¹⁴X. Li, M.-W. Lin, A. A. Puretzky, J. C. Idrobo, C. Ma, M. Chi, M. Yoon, C. M. Rouleau, I. I. Kravchenko, D. B. Geohegan, and K. Xiao, *Scientific Reports* **4**, 5497 (2014).
- ¹⁵C. S. Jung, F. Shojaei, K. Park, J. Y. Oh, H. S. Im, D. M. Jang, J. Park, and H. S. Kang, *ACS Nano* **9**, 9585 (2015).
- ¹⁶Y. Tang, W. Xie, K. C. Mandal, J. A. McGuire, and C. W. Lai, *Journal of Applied Physics* **118**, 113103 (2015).
- ¹⁷L. Karvonen, A. Säynätjoki, S. Mehravar, R. D. Rodriguez, S. Hartmann, D. R. T. Zahn, S. Honkanen, R. A. Norwood, N. Peyghambarian, K. Kieu, H. Lipsanen, and J. Riikonen, *Scientific Reports* **5**, 10334 (2015).
- ¹⁸X. Zhou, J. Cheng, Y. Zhou, T. Cao, H. Hong, Z. Liao, S. Wu, H. Peng, K. Liu, and D. Yu, *Journal of the American Chemical Society* **137**, 7994 (2015).
- ¹⁹D. J. Late, B. Liu, J. Luo, A. Yan, H. S. S. R. Matte, M. Grayson, C. N. R. Rao, and V. P. Dravid, *Advanced Materials* **24**, 3549 (2012).
- ²⁰N. C. Fernelius, *Prog. Crystal Growth and Charact* **28**, 275 (1994).
- ²¹K. Allakhverdiev. In *Proceedings of SPIE*, T. N. Dreischuh and A. T. Daskalova, editors, volume 8770, 877003, mar (2013).
- ²²S. I. Drapak, S. V. Gavrylyuk, Z. D. Kovalyuk, and O. S. Lytvyn, *Semiconductors* **42**, 414 (2008).
- ²³V. N. Katerynychuk, Z. R. Kudrynskyi, and Z. D. Kovalyuk, *Inorganic Materials* **50**, 339 (2014).
- ²⁴H. Iwakuro, C. Tatsuyama, and S. Ichimura, *Japanese Journal of Applied Physics* **21**, 94 (1982).
- ²⁵Z. Kovalyuk, V. Katerynychuk, A. Savchuk, and O. Lytvyn, *Superlattices and Microstructures* **44**, 416 (2008).
- ²⁶T. E. Beechem, B. M. Kowalski, M. T. Brumbach, A. E. McDonald, C. D. Spataru, S. W. Howell, T. Ohta, J. A. Pask, and N. G. Kalugin, *Applied Physics Letters* **107**, 173103 (2015).
- ²⁷D. Andres-Penares, A. Cros, J. P. Martínez-Pastor, and J. F. Sánchez-Royo, *Nanotechnology* **28**, 175701 (2017).
- ²⁸J. Susoma, J. Lahtinen, M. Kim, J. Riikonen, and H. Lipsanen, *AIP Advances* **7**, 015014 (2017).
- ²⁹S. Jandl, J. L. Brebner, and B. M. Powell, *Physical Review B* **13**, 686 (1976).
- ³⁰M. May, S. Debrus, K. Zakrzewska, H. Benisty, and A. Chevy, *Journal of the Optical Society of America B* **14**, 1048 (1997).
- ³¹R. M. Hoff, J. C. Irwin, and R. M. A. Lieth, *Canadian Journal of Physics* **53**, 1606 (1975).
- ³²T. J. Wieting and J. L. Verble, *Physical Review B* **5**, 1473 (1972).
- ³³E. Finkman, J. Tauc, R. Kershaw, and A. Wold, *Physical Review B* **11**, 3785 (1975).
- ³⁴A. Yamada, N. Kojima, K. Takahashi, T. Okamoto, and M. Konagai, *Japanese Journal of Applied Physics* **31**, 186 (1992).
- ³⁵A. Märkl, M. von der Emde, C. Nowak, W. Richter, and D. Zahn, *Surface Science* **331**, 631 (1995).
- ³⁶A. Anderson, A. Sanders, and W. Smith, *Journal of Raman Spectroscopy* **31**, 403 (2000).
- ³⁷N. J. Brassington, H. G. M. Edwards, and V. Fawcett, *Spectrochimica Acta Part A: Molecular Spectroscopy* **43**, 451-454 (1987).
- ³⁸O. A. Balitskii, V. P. Savchyn, and V. O. Yuhymchuk, *Semiconductor Science and Technology* **17**, L1 (2002).
- ³⁹P. J. Carroll and J. S. Lannin, *Solid State Communications* **40**, 81 (1981).
- ⁴⁰A. Baganich, V. Mikla, D. Semak, A. Sokolov, and A. Shebanin, *Phys. Stat. Sol.* **166**, 297 (1991).
- ⁴¹G. Lucovsky, A. Mooradian, W. Taylor, G. B. Wright, and R. C. Keezer, *Solid State Communications* **5**, 113 (1967).
- ⁴²V. V. Poborchii, A. V. Kolobov, and K. Tanaka, *Applied Physics Letters* **72**, 1167 (1998).
- ⁴³K. Ishida and K. Tanaka, *Physical Review B* **56**, 206 (1997).
- ⁴⁴T. Onuma, S. Fujioka, T. Yamaguchi, Y. Itoh, M. Higashiwaki, K. Sasaki, T. Masui, and T. Honda, *Journal of Crystal Growth* **401**, 330 (2014).
- ⁴⁵D. Dohy, G. Lucazeau, and A. Revcolevschi, *Journal of Solid State Chemistry* **45**, 180 (1982).
- ⁴⁶O. Balitskii and V. Savchyn, *Materials Science in Semiconductor Processing* **7**, 55 (2004).
- ⁴⁷Y. Stakhira and N. Tovstyuk, *Materials Science and Engineering: B* **116**, 112 (2005).
- ⁴⁸N. Berchenko, O. Balitskii, R. Lutsiv, V. Savchyn, and V. Vasylyts, *Materials Chemistry and Physics* **51**, 125 (1997).
- ⁴⁹H. H. Tippins, *Physical Review* **140**, A316 (1965).
- ⁵⁰A. Favron, E. Gaufres, F. Fossard, A.-L. Phaneuf-L'Heureux, N. Y.-W. Tang, P. L. Levesque, A. Loiseau, R. Leonelli, S. Francoeur, and R. Martel, *Nat Mater* **14**, 826 (2015).